Journal of
Composites Science

MDPI

Article

Effect of Heat-Shrinkable Tape Application on the Mechanical Performance of CFRP Components Obtained by a Filament Winding Process

Iacopo Bianchi [1], Archimede Forcellese [1], Tommaso Mancia [2], Chiara Mignanelli [1], Michela Simoncini [1,*] and Tommaso Verdini [1]

[1] Department of Industrial Engineering and Mathematical Sciences, Università Politecnica delle Marche, Via Brecce Bianche 12, 60131 Ancona, Italy; i.bianchi@pm.univpm.it (I.B.); a.forcellese@staff.univpm.it (A.F.); c.mignanelli@pm.univpm.it (C.M.); t.verdini@pm.univpm.it (T.V.)
[2] Department of Theoretical and Applied Sciences, Università degli Studi eCampus, Via Isimbardi 10, 22060 Novedrate, Italy; tommaso.mancia@uniecampus.it
* Correspondence: m.simoncini@staff.univpm.it; Tel.: +39-071-2204443

Abstract: Carbon Fiber Reinforced Polymers (CFRPs) are widely used in aerospace, automotive, and other sectors for their high strength-to-weight ratio and adaptability. In order to reach high mechanical performance and quality for CFRP components in which a thermosetting resin is used, the curing process plays a key role, and the optimal conditions have to be identified. In this context, the present study aims to study the effect of heat-shrinkable tape application on the mechanical performance of CFRP tubular components obtained by a filament winding process. To this purpose, CFRP hoop-wound components were realized with a laboratorial filament winding machine. Half of them were directly cured in a muffle oven, while the other half were cured after the application of heat-shrinkable tape around the external surface of the component. To evaluate the effect of the heat-shrinkable tape use on the mechanical properties of the CFRP wound parts, ring specimens, obtained by the tubular components according to the ASTM D2290 standard, were subjected to ring tensile tests. The thickness uniformity and void content of the components were evaluated by means of X-ray computed tomography, whilst the fracture surfaces were observed using scanning electron microscopy. It was demonstrated that the heat-shrinkable tape application around the external surface of the CFRP tubular components allows for improved mechanical performance of the wound parts due to the enhanced material compaction, resulting in stronger and more cohesive structures characterized by a uniform thickness and reduced void content.

Keywords: filament winding; CFRP; heat-shrinkable tape application; ring tensile test; tomography; SEM

Citation: Bianchi, I.; Forcellese, A.; Mancia, T.; Mignanelli, C.; Simoncini, M.; Verdini, T. Effect of Heat-Shrinkable Tape Application on the Mechanical Performance of CFRP Components Obtained by a Filament Winding Process. *J. Compos. Sci.* **2024**, *8*, 535. https://doi.org/10.3390/jcs8120535

Academic Editor: Jiadeng Zhu

Received: 19 November 2024
Revised: 8 December 2024
Accepted: 9 December 2024
Published: 16 December 2024

1. Introduction

Composite materials have been gaining increasing interest in the last years in many industrial sectors due to their high mechanical properties and low weights [1,2]. Among the various categories of composite materials, Carbon Fiber Reinforced Polymers (CFRPs) are the most widely used for automotive, aerospace, nautical, biomedical, and construction applications [3–5]. CFRPs allow us to realize high-performance components with a weight reduction with respect to traditional and conventional materials [6].

Over the years, many production processes have been developed to realize CFRP components, and the most used to produce axisymmetric components is the filament winding (FW) process. This technique allows us to realize composite tubular structures, which can be tailored in a wide range of properties; thus, they are suitable for several applications [7], especially in the aerospace sector and other critical sectors like pressure vessels, rocket engines, and aircraft structural components [8–11].

The FW process consists of the winding of the composite material around a rotating mandrel [12,13]. Depending on the kind of composite material used, the FW process can be classified in terms of wet-FW and dry-FW. The first one involves the use of dry continuous fibers, which enter a resin bath, by passing through a tension system, and then they are wounded around the mandrel [14]. The second one involves the use of preimpregnated fibers, which are directly wounded around the rotating mandrel, avoiding the passage in the resin bath, which is usually a critical step since it could lead to defects in the components [15].

The control of different axis speeds (e.g., mandrel and deposition head rotation, carriage, and cross-carriage translation) joined to a deposition head employed to lay down the prepregged or already impregnated fibers on the mandrel allows us to accurately define the material directions [10].

By winding the fibers with specific winding angles and following a precise path, high-performance and tailored structures can be realized. Indeed, the winding angle definition, which coincides with the fiber orientation direction, is crucial for the mechanical properties of the component since it is well known that composites' properties are greater along the direction of the fiber orientation. Thus, it is appropriate, during the design phase, to choose a winding angle that involves the fiber orientation along the load directions to obtain a high-performance composite component [16,17].

Commercially, different kinds of FW machines equipped with different configurations and numbers of numerically controlled axes can be found, which are suitable for producing complex-shaped structures. This technology avoids the labor-intensive and costly phases of traditional composite manufacturing methods by fully automating the lay-up process [18]. This also results in a reduction in the cost of composite products, making them more competitive in the market. The FW process requires a subsequent curing phase, which is crucial to consolidating the material. Most composite industries consider the autoclave curing process as the highest quality process for preimpregnated components [19,20]. Since the costs associated with the use of an autoclave are very high, several solutions can be considered to cure composites, such as oven curing, microwave curing, and the in situ process, as proved by the scientific literature [21–23].

The curing process plays a key role in the mechanical properties and the quality of a composite component; for this reason, it is important to identify which is the optimal solution to apply with respect to the applications. Therefore, in the scientific literature, there are several studies concerning this issue. As an example, Liang et al. [24] investigated the effect of the autoclave curing temperature on the mechanical properties of the composite material for the FW process, through tests performed on a pressure vessel. Betz et al. [25] studied the technical and economic aspects related to a microwave curing process for composite components obtained via FW. Moreover, Tabuchi et al. [26] investigated the influence of simultaneous heating for the curing process on the residual stress of the CFRP hoop-wound composite component. In addition, due to the high costs related to the autoclave curing process, the use of heat-shrinkable tape (HT) during oven curing processes gained a relevant interest; for this reason, some scientific literature studies concern the use of heat-shrinkable tapes during a consolidation process. Purnomo et al. [27] compared different finishing techniques, including the use of heat-shrinkable tape during the curing process of CFRP wound components, to investigate the surface quality of the obtained parts in terms of roughness, tensile stress, and stiffness. Heusinger et al. [28] investigated the effect of the number of shrink tape layers applied during an oven curing process, the shrink tape tension, and the holding time on the mechanical properties of a CFRP thermoplastic matrix tubular component.

Unfortunately, no studies concerning the effect of the heat-shrinkable tape application before the curing process on the mechanical properties and the surface quality in terms of thickness uniformity and of the CFRP thermosetting matrix wound component are available in the scientific literature.

In this context, this study aims to study the mechanical properties, the thickness uniformity, and the presence of voids of tubular hoop-wound CFRP components realized by means of the FW process. For this purpose, an X-WINDER machine was used to realize the CFRP hoop-wound components. Half of them were directly cured using a muffle furnace, while the other half of the wound parts were cured after the application of the heat-shrinkable tape around the external surface of the components. Then, cutting operations were performed to obtain ring specimens from the CFRP tubular parts obtained with and without HT. According to the D2290 ASTM standard, ring tensile tests were carried out at room temperature to evaluate the effect of the heat-shrinkable tape application on the mechanical properties of the CFRP hoop-wound components. Finally, X-ray computed tomography and scanning electron microscopy were used, respectively, to analyze the thickness uniformity and void content of the tubular components and the fracture surfaces of ring specimens obtained using the two different conditions.

The paper is organized as follows: after the Introduction, Section 2 defines the materials and methods used for this study, Section 3 shows the results and discussion; then, the Conclusions are drawn.

2. Materials and Methods

2.1. Materials

The composite tubular components were produced by means of a filament winding process using a towpreg consisting of carbon fibers (CF) as reinforcements and an epoxy resin matrix. The towpreg, composed of 30K CF filaments with a diameter of 7 μm, is characterized by a total width and thickness equal to 8 mm and 0.2 mm, respectively. The epoxy resin used in the present research (Huntsman International LLC) is characterized by a gel temperature (T_{gel}) equal to 90 °C and a glass transition temperature (T_g) of 120 °C.

The mechanical properties of the composite were calculated from the constituent data sheets using a mixture rule [29]. Table 1 reports the mechanical properties of the constituent materials and composite materials.

Table 1. Mechanical properties of CF, epoxy resin from data sheet, and CFRP calculated by using the mixture rule.

	Carbon Fiber	Epoxy Resin	Composite Material
Elastic modulus (E)	230 GPa	3.5 GPa	75 GPa
Ultimate Tensile Strength (UTS)	4900 MPa	73 MPa	750 MPa
Density (ρ)	1.8 g/cm^3	1.1 g/cm^3	1.5 g/cm^3

2.2. Filament Winding and Curing Processes

The X-winder (Arroyo Seco, NM, USA) laboratorial filament winding machine (Figure 1) was used to produce the CFRP tubular components. The machine has 4 controlled axes: the *X*-axis allows the movement of the cross carriage toward the rotating mandrel, the *Z*-axis allows the movement of the carriage along the longitudinal section of the mandrel, the W-axis allows the rotation of the mandrel around the *Z*-axis, and the U-axis allows the rotation of the deposition head around the *X*-axis. The controlled axes make it possible to wind the rotating mandrel. In particular, the X-axis is used to cover the domes of a vessel, the Z- and U-axes are used to cover the cylindrical section, and the W-axis is used to rotate the mandrel. The total movement and angle of fiber deposition is given by the combination of the translational movement of the deposition head and the rotational movement of the mandrel around its axis.

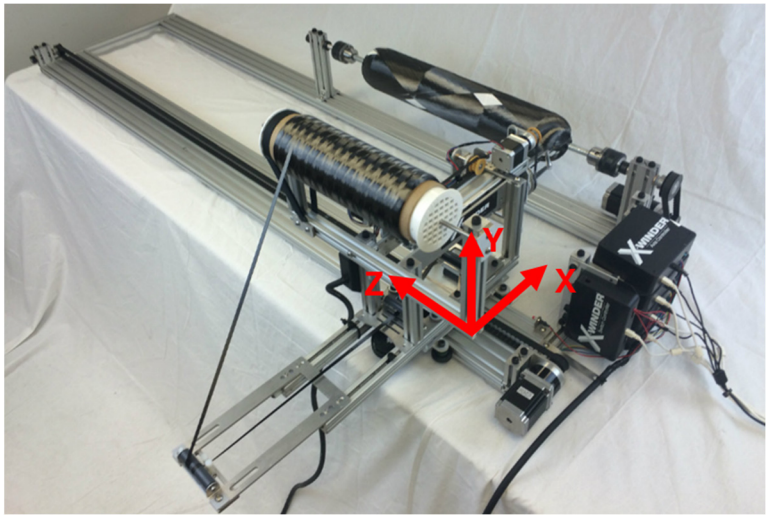

Figure 1. X-Winder filament winding machine.

In this study, the composite tubular components were obtained by winding three layers with a theoretical winding angle of 88° and carriage and mandrel maximum speeds of 101.60 mm/s and 3.14 rad/s, respectively.

The composite wound parts were then cured in a FALC muffle furnace 8.2 Lt—FM 8.2 (Treviglio, Bergamo, Italy), which allows for a maximum temperature of 1200 °C. According to the resin manufacturer, the curing process requires heating the chamber to 120 °C for 2 h. After curing, a post-cure is required to ensure all the resin is cured, at 150 °C for 2 h, followed by air cooling. Figure 2 shows the curing and post-cure cycle.

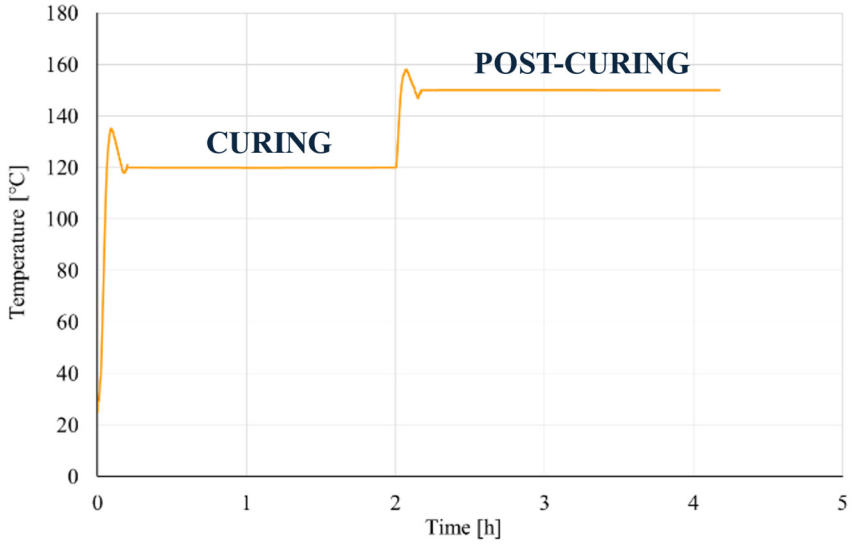

Figure 2. Composite part curing and post-curing cycle.

In order to investigate different curing conditions, half of the CFRP wound components were directly cured in the muffle furnace, while the other half of the wound parts were cured after the application of a heat-shrinkable tape (DIATEX SAS, Saint-Genis-Laval, France) around the external surface of the component. The heat-shrinkable tape is a tape that exerts a compressive force on the CFRP's underlying structure when heat is applied during the curing process. Furthermore, the tape is entirely adhesive free, so once the curing process is completed, the tape can be easily removed with no residue left behind.

Figure 3 shows the wound tubular components after curing, obtained with and without the application of the tape before the curing process.

Figure 3. CFRP wound tubular components obtained: (**a**) without and (**b**) with heat-shrinkable tape application before curing process.

2.3. X-Ray Computed Tomography and Scanning Electron Microscopy

An important issue of the FW process is related to the thickness uniformity both along the tubular component section and width and the presence of voids due to the winding strategy or process defects. For these reasons, in the present work, an X-ray computed tomography (X-CT) scan was performed using a Zeiss METROTOM 1500 CT (Zeiss, Oberkochen, Germany) system equipped with an X-ray tube with a minimum focal spot of 7 μm, a maximum accelerating voltage of 199 kV, and a maximum current leakage of 1000 μA. The source–detector distance was maintained at 1500 mm, with a maximum measuring range of 350 mm × 300 mm and a detector resolution of 2048 × 2048 pixels.

The different slices of the specimens for the investigated conditions, obtained by means of a scanning process performed with X-CT, were analyzed using National Instrument (NI) Vision Suite 2023 software. For each slice, eight benchmarks were considered along the circular section to analyze the thickness uniformity along the transversal direction, both for the specimens cured with and without the HT (Figure 4). In addition, the thickness uniformity along the longitudinal direction of the specimens was evaluated by analyzing two different slices for each specimen, obtained both with and without heat-shrinkable tape, at about a distance of 10 mm.

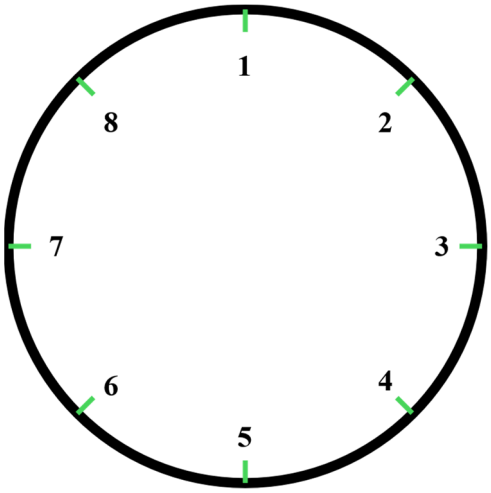

Figure 4. The eight benchmarks considered for the evaluation of specimen thickness distribution.

In addition, to achieve high-resolution imaging of the fractured surfaces of the ring specimens after tensile tests, the TESCAN VEGA 3 (TESCAN, Brno, Czech Republic) was used for a scanning electron microscopy (SEM) investigation. Before SEM analysis, the fracture surface of the samples was nanocoated with gold to have better electrical transmission during observation.

2.4. Tensile Test of Ring Specimens

The mechanical properties of the CFRP filament wound components, obtained with or without the application of an HT before the curing process, were analyzed by means of ring tensile tests performed according to ASTM D2290 [30] using a servo-hydraulic testing machine (MTS 810®, MTS Systems Corporation, Eden Prairie, MN, USA) equipped with a 250 kN load cell (Figure 5). During tests, the crosshead speed was kept constant at 0.1 mm/s. The experimental results were plotted as applied load versus displacement curves from which the hoop tensile strength (HTS) was evaluated.

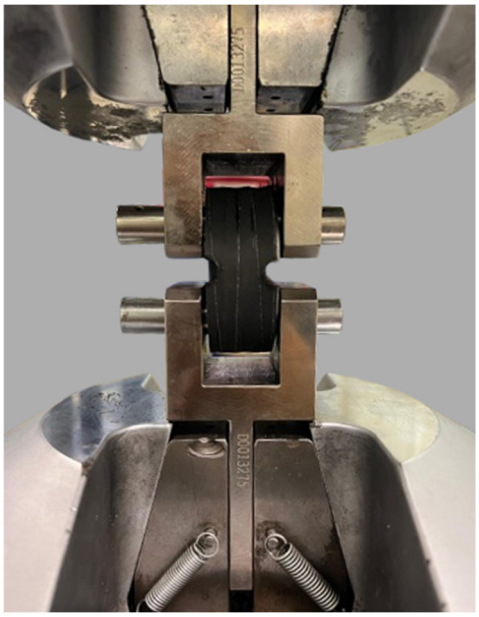

Figure 5. Tensile test of ring specimens.

In accordance with the ASTM D2290 [30] standard, Procedure A was considered to test the specimens as it is suitable for a thermoset composite ring. The rings were obtained from the composite tubular components by means of drilling and cutting operations. Five specimens, obtained both using and not using the HT, were realized and tested to obtain a reliable average test value. Specimen dimensions are reported in Figure 6.

The split disc test from ASTM D2290 [30] is used to evaluate the circumferential properties of filament wound products. Several factors have a significant effect on the results of the test. The hoop tensile strength calculation does not take into account the bending component during the test, resulting in a reduction in HTS of up to 25% [31]. Friction between the specimen and fixture disc can affect the stress/strain distribution along the circumference of the disc; in particular, the effect increases with increasing friction values [32–37].

From the results of the tensile tests, it is possible to calculate the HTS according to the standard and assuming a uniform tensile stress in the ring cross-section by using Equation (1):

$$\sigma_{HTS} = \frac{P}{2 \cdot A_{min}} \quad (1)$$

in which P [kN] is the maximum load during the tensile test and A_{min} [mm^2] is the minimum area between the two reduced sections.

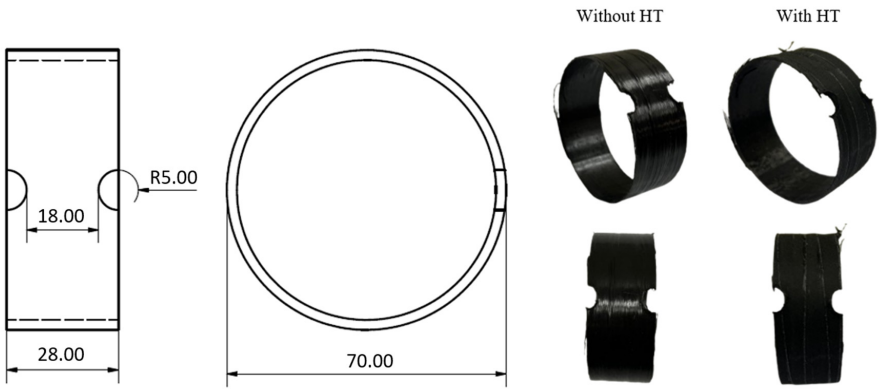

Figure 6. Ring specimen dimensions according to ASTM D2290 standard.

Since the weight can vary depending on the application or not of the heat-shrinkable tape, the specific strength and specific modulus were calculated by dividing the HTS by the weight of the specimens.

3. Results and Discussion

In order to evaluate the effect of the heat-shrinkable tape application on the mechanical properties of the CFRP wound parts, ring specimens, obtained from the tubular components by machining operations, were subjected to ring tensile tests. Figure 7 shows the tomography of typical rings obtained both using and not using the HT before the curing process. Specifically, two different slices (i.e., slice 100 and slice 200) of two typical ring specimens can be observed.

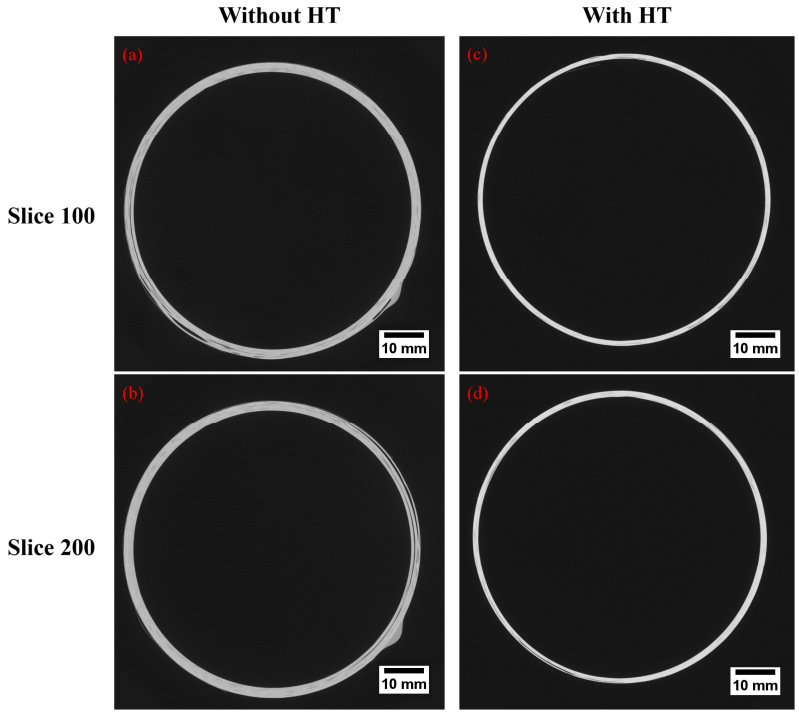

Figure 7. X-ray computed tomography images of typical ring specimens obtained from cured wound components: (**a**) without HT—slice 100, (**b**) without HT—slice 200, (**c**) with HT—slice 100, and (**d**) with HT—slice 200.

By comparing the ring specimens obtained with and without the application of the heat-shrinkable tape, a high quantity of voids can be clearly observed in the specimen obtained without HT (Figure 7a,b) as compared to that obtained using the heat-shrinkable tape (Figure 7c,d), irrespective of the X-CT slice taken into account. Such a result can be attributed to the capability of the heat-shrinkable tape to guarantee a high level of compaction of the underlying layers when it is heated. Furthermore, the application of the HT allows a good distribution of the epoxy resin on the component. As a matter of fact, the ring specimen obtained without the application of HT (Figure 7a,b) is characterized by the presence of superficial resin drops. Such a drawback occurs when the epoxy resin reaches the low viscosity point, moves along the circular section, and accumulates below the wound tubular component in the form of drops, due to gravity.

In addition to the improved compaction of the wrapped material by FW and the void reduction, the presence of the heat-shrinkable tape allows for benefits in terms of uniformity of the thickness of the wound components. As a matter of fact, Figure 7 also shows that the thickness of the ring specimen cured with the HT (Figure 7c,d) is lower than the one related to the specimen cured without HT (Figure 7a,b).

According to the experimental procedure described in Section 2.4, the thicknesses of the ring specimens, obtained using and not using HT, were measured by considering the eight benchmarks along the circular section at two different X-CT slices along the width. To this purpose, the two ring specimens, obtained with and without HT, respectively, were analyzed at the same X-CT slice using NI Vision software (Figure 8).

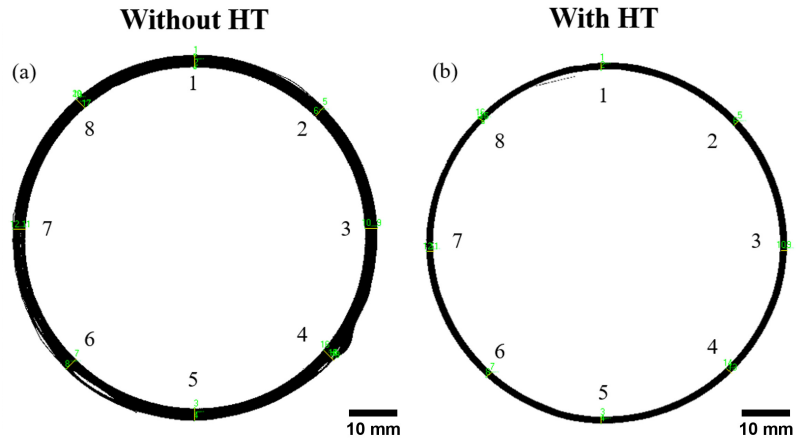

Figure 8. Comparison between the two ring specimens, analyzed at the same X-CT slice using NI Vision software, obtained: (**a**) without HT and (**b**) with HT (X-CT slice n. 100).

For a given X-CT slice, the specimens cured with the HT application are characterized by lower thickness values in all the benchmark points as compared to those cured without HT, denoting an effective compaction of CFRP layers due to the presence of the heat-shrinkable tape (Figure 9). Specifically, the reduction in mean specimen thickness is about 45% (in particular, 49% as Slice 100 is considered and about 42% in Slice 200). To this purpose, Table 2 summarizes the mean thickness values measured in the eight benchmark points of the ring specimens obtained with and without the HT application before the curing process. The mean thickness was calculated both along the circular section and the width of the ring specimens. The standard deviation of the thickness values with respect to the mean values was evaluated as well. Specifically, the standard deviation along the circular section of the ring specimens without HT is higher than that obtained from specimens with HT.

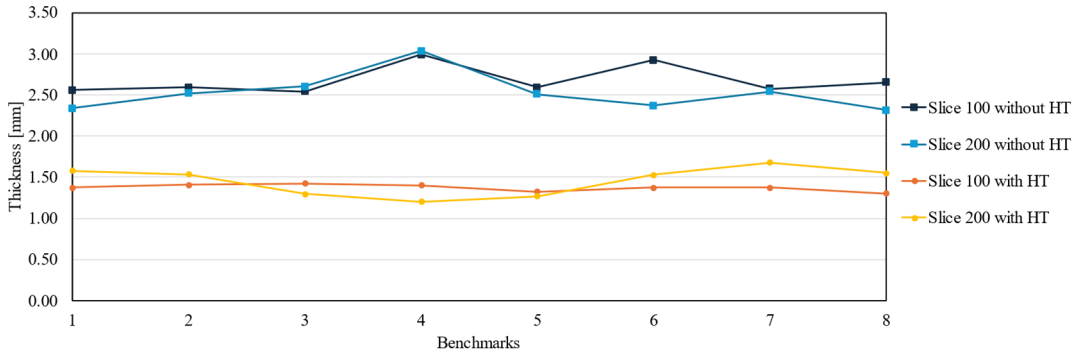

Figure 9. Thickness distribution, evaluated at two different X-CT slices, in ring specimens obtained with and without heat-shrinkable tape.

Table 2. Thickness values measured in the eight benchmark points of the ring specimens obtained with and without the HT application, mean thickness, and standard deviation values.

Benchmarks	Thickness [mm]			
	Slice 100		Slice 200	
	Without HT	With HT	Without HT	With HT
1	2.56	1.37	2.34	1.58
2	2.59	1.41	2.52	1.54
3	2.54	1.42	2.60	1.30
4	2.99	1.40	3.04	1.21
5	2.59	1.32	2.51	1.27
6	2.92	1.38	2.37	1.53
7	2.58	1.38	2.54	1.68
8	2.65	1.30	2.32	1.55
Mean (section)	2.68	1.37	2.53	1.46
Standard Deviation (section)	0.18	0.04	0.23	0.17
	Without HT		With HT	
Mean (width)	2.60		1.41	
Standard Deviation (width)	0.18		0.08	

As far as the thickness along the width is concerned, by comparing the thickness values measured at the two different slices of the same ring specimen, Figure 9 also shows that the ring specimens' thickness along the width of the components is significantly variable for specimens cured without HT, whilst a more uniform thickness distribution can be observed in ring specimens obtained using the HT. In particular, the mean thickness value of the specimen cured without HT is higher than the one of the specimens cured with HT by about 84%, with a standard deviation along the width higher for the specimen cured without HT than the one cured with HT. Such results demonstrate that the heat-shrinkable tape application before the curing process leads to a reduction in the mean thickness values and to an improvement in the thickness distribution both along the circular section and the width.

In order to evaluate the effect of heat-shrinkable tape application on the mechanical properties of the CFRP tubular components obtained by means of FW, ring tensile tests were performed at room temperature. According to ASTM standard D2290, the hoop tensile stress was evaluated as a function of the crosshead displacement, both for specimens with and without HT. The hoop tensile strength (σ_{HTS}) was obtained as the maximum value of the hoop tensile stress behavior. Table 3 summarizes the σ_{HTS} and the maximum load values obtained by the ring tensile tests. Moreover, in order to investigate the specific hoop tensile strength and the specific load, the ratio between the hoop tensile strength and weight and the one between the load and the weight, reported in Table 3, were considered.

Table 3. Typical values obtained by the tensile tests.

	Without Heat-Shrinkable Tape	With Heat-Shrinkable Tape
σ_{HTS} [MPa]	646.26	1473.28
Weight [g]	18.34	12.11
Specific σ_{HTS} [MPa/g]	35.24	121.66
Load [kN]	48.86	71.60
Specific load [kN/g]	2.66	5.91

The effect of the heat-shrinkable tape application on the typical specific load versus crosshead displacement curves and specific hoop tensile stress versus crosshead displacement curves is shown in Figure 10.

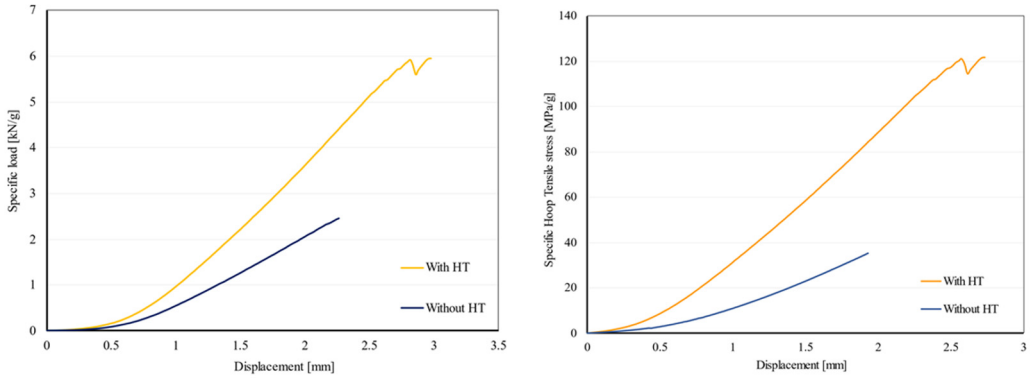

(a) (b)

Figure 10. (**a**) Typical specific load versus crosshead displacement curves and (**b**) specific hoop tensile stress versus crosshead displacement curves obtained by testing the ring specimens obtained with and without HT.

Irrespective of the heat-shrinkable tape application, the specific load (Figure 10a) and, consequently, the specific hoop tensile stress (Figure 10b) increase with displacement until reaching a peak value at which the ring specimen fracture occurs. As far as the ring specimen with HT is considered, it can be observed that the specific load and the specific hoop tensile stress level reached by the specimen with HT are always higher than those of the specimens obtained without HT, denoting that the application of a heat-shrinkable tape before the curing process involves an improvement in the mechanical properties of the wound component. Specifically, it can be observed that the ring specimens with the heat-shrinkable tape achieved a specific load increase of about 55% with respect to the specimens without the application of the tape. As far as the specific hoop tensile stress is concerned, ring specimens obtained with HT achieve a specific HTS of about 121.66 MPa/g, which is about a 71% increase with respect to the 35.24 MPa/g obtained by specimens cured without the HT application. Furthermore, according to the scientific literature [7,38], a significant improvement in elongation can be observed in ring specimens with HT. To justify the results obtained by ring tensile tests in terms of the mechanical properties of tubular components, a scanning electron microscopy investigation was carried out to observe the fracture surfaces of ring specimens obtained with and without HT. Figure 11 shows a typical ring specimen obtained using the HT, fractured at the holes that represent stress concentration zones [39].

Figure 11. Typical ring specimen, obtained using the HT, fractured after tensile test.

Figure 12 shows SEM images of the fracture surfaces of ring specimens obtained both without (Figure 12a–c) and with (Figure 12d–f) heat-shrinkable tape at different magnifications. Irrespective of the application of heat-shrinkable tape on the external surface of tubular components before the curing process is concerned, it can be observed that the CFRP specimens are characterized by a brittle fracture. During ring tensile tests, failure begins with transverse microcracks. As the stress level further increases, in particular, corresponding to the holes in the specimens, the number of transverse microcracks increases until saturation is reached. Delamination, fiber failure, and longitudinal cracking can follow transverse crack formation. In the present study, after transverse microcracking, a marked delamination between CFRP layers appears in the ring specimens. The delamination can occur on several adjacent layers, and therefore, the debonding surface can appear as a flat stepped surface (Figure 12a,d).

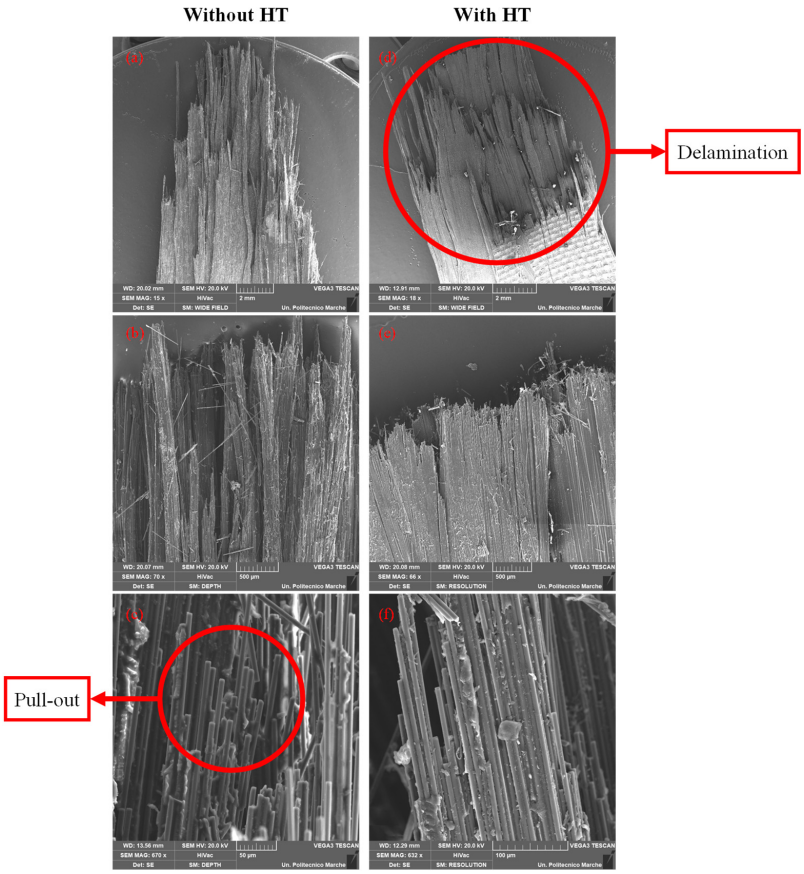

Figure 12. SEM images of the fracture surfaces of ring specimens obtained: (**a**–**c**) without HT and (**d**–**f**) with HT at different magnifications.

As far as the effect of heat-shrinkable tape application is concerned, it can be noted that the ring specimen obtained without HT (Figure 12a) is characterized by more unbound, less compacted, and more frayed fibers than those in the ring specimen obtained using the HT (Figure 12d). Such results can be attributed to the effective compaction of CFRP layers due to the heat-shrinkable tape application, shown in the X-CT images of Figure 7 and in the thickness distribution of Figure 9.

Furthermore, Figure 12d shows that the external surface layer of the ring, on which the tape has been wrapped, is characterized by a typical texture due to the compressive force exerted by the HT on the component during the curing process. Finally, the surface finish of the component will be characterized by a high roughness, which is suitable for any subsequent surface processing.

At a higher magnification (Figure 12b,e), the comparison between the fracture surfaces of the specimens highlights that, in the sample obtained by applying the heat-shrinkable tape, the fibers maintain their position in an orderly manner, as they are more bound to the matrix. This result is due to the presence of the HT, which during the curing process, contracts, ensuring a high level of compaction and greater adhesion at the fiber–matrix interface. This provides a greater capacity for the fibers to remain bound to the matrix during fracture. Figure 12c shows the presence of many dry fibers and very poor epoxy resin quantity; the amount of resin in the ring specimen obtained without the HT application is much lower than the one that can be observed in Figure 12f. This proves that a pull-out of fibers occurs during the fracture of the specimen obtained without HT. On the contrary, Figure 12f shows that many fibers are still bonded due to the matrix presence. Finally, Figure 13 shows a typical matrix cracking that occurs due to its relatively low strength in the loading direction.

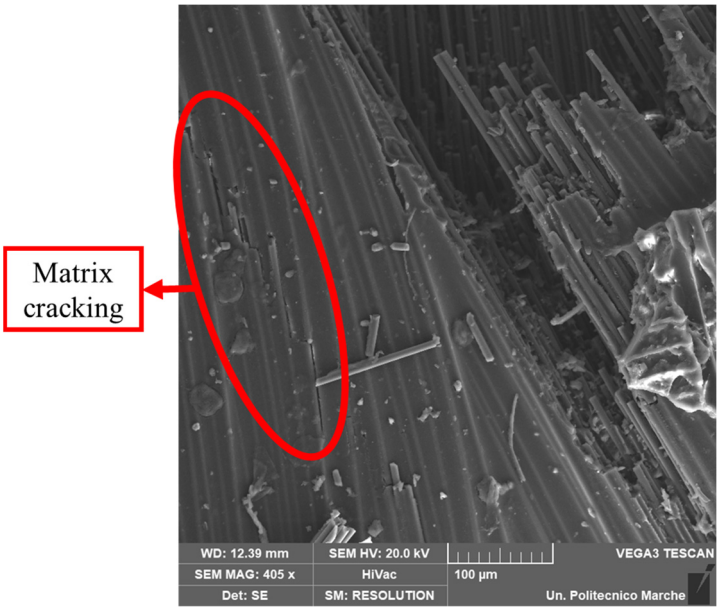

Figure 13. SEM image of the fracture surfaces of a ring specimen obtained with HT in which the matrix cracking can be observed.

In conclusion, it can be stated that the application of heat-shrinkable tape before the polymerization process of a CFRP-wrapped component improves the compaction of the material and the adhesion at the fiber–matrix interface, reduces the void content, and optimizes the thickness distribution of the tubular component. These benefits result in a significant improvement in the mechanical properties of the CFRP tubular component under tensile stress.

4. Conclusions

The present investigation aimed at studying the effect of heat-shrinkable tape application on the mechanical properties, thickness distribution, and void presence of CFRP hoop-wound components realized with a laboratorial filament winding machine. Half of the components were directly cured in a muffle oven, while the other half were cured after the application of heat-shrinkable tape around the external surface of the part. Ring tensile tests were then performed at room temperature on ring specimens manufactured by the tubular components according to the ASTM D2290 standard. The thickness distribution and void content of the components were evaluated using X-ray computed tomography, whilst the fracture surfaces were observed using scanning electron microscopy.

The main results can be summarized as follows:

- The X-CT shows that the heat-shrinkable tape application on the external surface of the CFRP tubular component involves a significant thickness reduction of about 45%. Furthermore, the HT application resulted in improved thickness distribution both along the circular cross-section of the component and across the width of the specimens, compared to the tubular component cured without HT.
- X-ray tomography shows a significant decrease in void content in the ring specimens cured with the presence of heat-shrinkable tape, indicating an improved resin distribution and reduction in defects. This contributes to improving the structural integrity of the CFRP components.
- Tensile tests show that the specific hoop tensile stress increases with displacement until reaching a peak value at which the ring specimen fracture occurs.
- Ring specimens obtained with heat-shrinkable tape exhibit a specific load of about 55% higher than the samples without the application of the tape. Furthermore, they achieve a specific hoop tensile strength of about 121.66 MPa/g, which is about 71% increased with respect to the 35.24 MPa/g obtained by specimens cured without the HT application. These results show the effectiveness of the heat-shrinkable tape in improving material compaction.
- The SEM observation shows that specimens with HT application exhibit more orderly fracture surfaces and stronger fiber–matrix bonding, whereas those obtained without HT show frayed fiber surfaces and significant fiber pull-out.
- The application of heat-shrinkable tape before the curing process improves the compaction of the material and the adhesion at the fiber–matrix interface, resulting in a significant improvement in the mechanical properties of the CFRP tubular component under tensile stress.

Future works will concern the variation in the types of tape and other parameters during the curing process and the number of layers of the winding to further optimize the mechanical performance of CFRP components. In addition, the potential of other curing tools, such as microwave-assisted tools or an autoclave, could be evaluated to provide insights into achieving higher quality and efficiency in CFRP manufacturing for high-performance applications.

Author Contributions: Conceptualization, A.F. and M.S.; methodology, I.B., C.M., T.M. and T.V.; software, I.B., C.M., T.M. and T.V.; validation, I.B., C.M., T.M. and T.V.; formal analysis, I.B., C.M., T.M., M.S. and T.V.; investigation, I.B., C.M., T.M. and T.V.; resources, A.F. and M.S.; data curation, I.B., C.M., T.M. and T.V.; writing—original draft preparation, I.B., C.M., T.M. and T.V.; writing—review and editing, A.F. and M.S.; visualization, I.B., C.M., T.M. and T.V.; supervision, A.F. and M.S.; project administration, A.F. and M.S. All authors have read and agreed to the published version of the manuscript.

Funding: This research received no external funding.

Data Availability Statement: The original contributions presented in the study are included in the article, further inquiries can be directed to the corresponding author.

Conflicts of Interest: The authors declare no conflicts of interest.

References

1. Holmes, M. Carbon composites continue to find new markets. *Reinf. Plast.* **2017**, *61*, 36–40. [CrossRef]
2. Cepero-Mejías, F.; Phadnis, V.A.; Kerrigan, K.; Curiel-Sosa, J.L. A finite element assessment of chip formation mechanisms in the machining of CFRP laminates with different fibre orientations. *Compos. Struct.* **2021**, *268*, 113966. [CrossRef]
3. Rubino, F.; Nisticò, A.; Tucci, F.; Carlone, P. Marine Science and Engineering Marine Application of Fiber Reinforced Composites: A Review. *J. Mar. Sci. Eng.* **2020**, *8*, 26. [CrossRef]
4. Singh, P.; Raghavender, V.; Joshi, S.; Vasant, N.P.; Awasthi, A.; Nagpal, A.; Jasim Abd al-saheb, A. Composite material: A review over current development and automotive application. *Mater. Today Proc.* **2023**, *in press*. [CrossRef]
5. Henning, F.; Kärger, L.; Dörr, D.; Schirmaier, F.J.; Seuffert, J.; Bernath, A. Fast processing and continuous simulation of automotive structural composite components. *Compos. Sci. Technol.* **2019**, *171*, 261–279. [CrossRef]
6. Kelly, J.C.; Sullivan, J.L.; Burnham, A.; Elgowainy, A. Impacts of Vehicle Weight Reduction via Material Substitution on Life-Cycle Greenhouse Gas Emissions. *Environ. Sci. Technol.* **2015**, *49*, 12535–12542. [CrossRef]
7. Eggers, F.; Almeida, J.H.S.; Azevedo, C.B.; Amico, S.C. Mechanical response of filament wound composite rings under tension and compression. *Polym. Test.* **2019**, *78*, 105951. [CrossRef]
8. Krikanov, A.A. Composite pressure vessels with higher stiffness. *Compos. Struct.* **2000**, *48*, 119–127. [CrossRef]
9. Iacopo, B.; Chiara, M.; Michela, S.; Tommaso, V. Life cycle analyses of a composite towbar realized via filament winding and comparison with traditional metallic alternatives. *Sustain. Mater. Technol.* **2024**, *40*, e00980. [CrossRef]
10. Bianchi, I.; Forcellese, A.; Galliani, F.; Greco, L.; Mignanelli, C.; Trevisan, G. Process and structural simulation for the development of a pressure vessel through filament winding technology. *Mater. Res. Proc.* **2023**, *28*, 347–556. [CrossRef]
11. Mignanelli, C.; Bianchi, I.; Forcellese, A.; Simoncini, M. Life cycle assessment of pressure vessels realized with thermoplastic and thermosetting matrix composites. *Int. J. Adv. Manuf. Technol.* **2024**, *135*, 4491–4509. [CrossRef]
12. Mateen, M.A.; Shankar, D.V.R.; Hussain, M.M. Design and development of low cost two axis filament winding machine. *J. Adv. Manuf. Technol.* **2018**, *12*, 117–126.
13. Ma, Q.; Rejab, M.R.M.; Idris, M.S. Dataset of the lab-scale 3-axis winding machine integrated with the portable real-time winding angle measurement system. *Data Brief* **2022**, *45*, 108731. [CrossRef]
14. Carosella, S.; Hügle, S.; Helber, F.; Middendorf, P. A short review on recent advances in automated fiber placement and filament winding technologies. *Compos. B Eng.* **2024**, *287*, 111843. [CrossRef]
15. Alimirzaei, S.; Najafabadi, M.A.; Nikbakht, A. Investigation of Mechanical Properties and Failure Behavior of CFRP Filament-Wound Composites Using an Acoustic Emission-Based Methodology and Numerical Simulation. *Fibers Polym.* **2023**, *24*, 693–707. [CrossRef]
16. Annadorai, M.E.; Ramakrishna, M.; Jyothi, Y. Effect on mechanical properties of CFRP composites in different fiber orientations. *Interactions* **2024**, *245*, 1–11. [CrossRef]
17. Pathak, A.K.; Garg, H.; Subhedar, K.M.; Dhakate, S.R. Significance of Carbon Fiber Orientation on Thermomechanical Properties of Carbon Fiber Reinforced Epoxy Composite. *Fibers Polym.* **2021**, *22*, 1923–1933. [CrossRef]
18. Vita, A.; Castorani, V.; Germani, M.; Marconi, M. Comparative life cycle assessment and cost analysis of autoclave and pressure bag molding for producing CFRP components. *Int. J. Adv. Manuf. Technol.* **2019**, *105*, 1967–1982. [CrossRef]
19. Taser, M.K.H.H. Experimental investigation of the effect of fabric wrapping method and autoclave curing on the mechanical and thermal degradation of carbon nanotube doped and undoped carbon composite pipes. *Polym. Compos.* **2024**, *45*, 12885–12898. [CrossRef]
20. Stadler, H.; Kiss, P.; Stadlbauer, W.; Plank, B.; Burgstaller, C. Influence of consolidating process on the properties of composites from thermosetting carbon fiber reinforced tapes. *Polym. Compos.* **2022**, *43*, 4268–4279. [CrossRef]
21. Bao, H.; Marguerès, P.; Olivier, P. An innovative and low-cost system for in situ and real-time cure monitoring using electrical impedancemetry for thermoset and CFRP laminate. *Meas. Sci. Technol.* **2023**, *35*, 035603. [CrossRef]
22. Rao, S.; Revgade, S.V.; Manjunath, N.M.; Prakash, M.R. Microwave Assisted Curing of CFRP Composite Laminates for Aerospace Applications. In Proceedings of the 17th ISAMPE National Conference on Composites; Springer: Berlin/Heidelberg, Germany, 2024; Volume 39, pp. 131–138. [CrossRef]
23. Collinson, M.G.; Swait, T.J.; Bower, M.P.; Nuhiji, B.; Hayes, S.A. Development and implementation of direct electric cure of plain weave CFRP composites for aerospace. *Compos. Part A Appl. Sci. Manuf.* **2023**, *172*, 107615. [CrossRef]
24. Liang, J.; Liu, L.; Qin, Z.; Zhao, X.; Li, Z.; Emmanuel, U.; Feng, J. Experimental Study of Curing Temperature Effect on Mechanical Performance of Carbon. Fiber Composites with Application to Filament Winding Pressure Vessel Design. *Polymers* **2023**, *15*, 982. [CrossRef]
25. Betz, S.; Köster, F.; Ramopoulos, V. Energy and Time Efficient Microwave Curing for CFRP Parts Manufactured by Filament Winding. *Mater. Sci. Forum* **2015**, *825–826*, 741–748. [CrossRef]
26. Tabuchi, D.; Sajima, T.; Doi, T.; Onikura, H.; Ohnishi, O.; Kurokawa, S.; Miura, T. Residual Stress of Hoop-Wound CFRP Composites Manufactured with Simultaneous Heating. *Sens. Mater.* **2012**, *24*, 99–111.
27. Purnomo, H.; Soemardi, T.P.; Budiono, H.D.S.; Wibowo, H.B.; Ibadi, M. The Filament Winding Method's Finishing Process Impact on Highfidelity Specimens: Homogenity of Density, Fiber Volume Fraction, Outer Surface Roughness and Tensile Strength. *East. Eur. J. Enterp. Technol.* **2023**, *6*, 43–51. [CrossRef]

28. Von Heusinger, J.; Grohmann, Y.; Khan, S. Methods for the Post-Consolidation of High-Speed-Wound Thermoplastic CFRP Tubes. Available online: https://www.dlr.de/sy (accessed on 1 December 2024).
29. Jacquet, E.; Trivaudey, F.; Varchon, D. Calculation of the transverse modulus of a unidirectional composite material and of the modulus of an aggregate. Application of the rule of mixtures. *Compos. Sci. Technol.* **2000**, *60*, 345–350. [CrossRef]
30. *ASTM D2290-19a*; Test Method for Apparent Hoop Tensile Strength of Plastic or Reinforced Plastic Pipe. ASTM International: West Conshohocken, PA, USA, 2019. [CrossRef]
31. Lee, S.; Kim, S.H.; Kim, S.; Choi, J.; Choi, H.J. Hoop tensile strength of tubular carbon fiber reinforced silicon carbide matrix composites. *Ceram. Int.* **2018**, *44*, 17087–17093. [CrossRef]
32. Yoon, S.H.; Cho, W.M.; Kim, C.G. Measurement of modulus in filament wound ring specimen using split disk test. *Exp. Tech.* **1997**, *21*, 25–28. [CrossRef]
33. Perillo, G.; Vacher, R.; Grytten, F.; Sørbø, S.; Delhaye, V. Material characterisation and failure envelope evaluation of filament wound GFRP and CFRP composite tubes. *Polym. Test.* **2014**, *40*, 54–62. [CrossRef]
34. Chen, J.F.; Li, S.Q.; Bisby, L.A.; Ai, J. FRP rupture strains in the split-disk test. *Compos. B Eng.* **2011**, *42*, 962–972. [CrossRef]
35. Al Ali, I.B.K.F. A procedure to determine the tangential true stress-strain behavior of pipes. *Int. J. Press. Vessel. Pip.* **2015**, *128*, 59–68. [CrossRef]
36. Zhao, Y.; Druzhinin, P.; Ivens, J.; Vandepitte, D.; Lomov, S.V. Split-disk test with 3D Digital Image Correlation strain measurement for filament wound composites. *Compos. Struct.* **2021**, *263*, 113686. [CrossRef]
37. Khalfallah, A.; Ktari, Z.; Leitão, C.; Fernandes, J.V. New Mandrel Design for Ring Hoop Tensile Testing. *Exp. Tech.* **2021**, *45*, 769–787. [CrossRef]
38. Kaynak, C.; Erdiller, E.S.; Parnas, L.; Senel, F. Use of split-disk tests for the process parameters of filament wound epoxy composite tubes. *Polym. Test.* **2005**, *24*, 648–655. [CrossRef]
39. Abbasi, R.R.F. Numerical and Experimental Analyses of the Hoop Tensile Strength of Filament-Wound Composite Tubes. *Mech. Compos. Mater.* **2020**, *56*, 423–436. [CrossRef]